

# Rock Mass Modeling Approach for Simulating Wave Propagation, Rock Fracture, and Rock Ejection.

Raffaldi, M.J.

*National Institute for Occupational Safety and Health, Spokane, WA, USA*

Loken, M.C.

*M&K Consulting, Saint Paul, MN, USA*

Copyright 2016 ARMA, American Rock Mechanics Association

This paper was prepared for presentation at the 50<sup>th</sup> US Rock Mechanics / Geomechanics Symposium held in Houston, Texas, USA, 26-29 June 2016. This paper was selected for presentation at the symposium by an ARMA Technical Program Committee based on a technical and critical review of the paper by a minimum of two technical reviewers. The material, as presented, does not necessarily reflect any position of ARMA, its officers, or members. Electronic reproduction, distribution, or storage of any part of this paper for commercial purposes without the written consent of ARMA is prohibited. Permission to reproduce in print is restricted to an abstract of not more than 200 words; illustrations may not be copied. The abstract must contain conspicuous acknowledgement of where and by whom the paper was presented.

**ABSTRACT:** As part of an ongoing research effort to improve ground control safety in deep vein mines, researchers at the National Institute for Occupational Safety and Health (NIOSH), Spokane Mining Research Division (SMRD) have developed a simplistic approach to modeling dynamic behavior of rock using commercially available software. This methodology will be applied to study the behavior of underground excavations subjected to dynamic loading from remote seismic sources in order to better understand the relationship between seismic wave-parameters, rock mass damage, excavation stability, and ground-support demands. The potential exists to improve safety in burst prone ground through better understanding of the effects of seismic loads on excavations. This paper describes a preliminary one-dimensional investigation of the model that validates its performance and provides insight into the dynamic failure of rock. The main observation is that the dynamic stresses that develop in the rock near a free surface are different than those that occur within a constrained solid. In a constrained solid, the dynamic stresses are directly proportional to the velocity amplitude of the propagating wave. This study shows that in the vicinity of an unconstrained surface, the accelerations associated with a seismic wave are also important to understanding dynamic stress and rock ejection. As the wave passes, forces develop that are equal to the product of the mass and acceleration of the rock block attempting to eject. For a seismic wave of given peak particle velocity, higher frequencies will be associated with higher accelerations and have the potential to be more damaging to a rock surface. Increased use of dynamic modeling will develop knowledge of the effects of seismic loading on excavations and ground support and may lead to designs that better protect miners.

## 1. INTRODUCTION

In the last few decades there has been significant advancement in computing power and the capabilities of numerical modeling software for use in geomechanical problem solving. The ability to perform fully-dynamic simulations in geomechanics has never been more accessible or user friendly than it is today. However, practical application of this technology in rock engineering projects is not common place as of yet (compared with static modeling). Further development and increased use of this technology may provide significant insights into problems associated with mining induced seismicity and thereby help protect miners from the hazards associated with rockbursts.

Dynamic problems are particularly challenging because a full characterization of the initial static state can never be completely realized in geotechnical engineering, hindering the analysis from the start. Additionally, the strength and mechanical behavior of intact rock (Christensen et al., 1972; Qian et al., 2009; Johnson

2010), rock joints (Bakhtar and Barton, 1984; Barbero et al., 1996; Mohammed et al., 2006), and many ground-support materials (Ansell, 2005, 2006; Player et al., 2008) are dependent on loading rate. Moreover, their dynamic behavior is not well characterized. Lastly, the appropriate dynamic loading must be applied and adequate characterization of seismic loads is challenging.

In the case of an earthquake, the source mechanism may be hundreds of kilometers from the area of interest, and in this case, ground motion input to the base of the model is often appropriate. However, in the case of mining induced seismicity, the wave could approach the excavation from any angle, and the source event could be within a few meters of, or even coincide with rockburst damage. In this case, actual simulation of the source mechanism may be required, further complicating the analysis. Simulation of a natural event such as a fault slip is particularly challenging, though practical modeling work concerning simulating slip mechanisms has been performed by Sainokoi and Mitri (2014, 2015).

Additionally, the characteristics of source wave motion, and how it changes during propagation through the rock mass, is at this time not well understood. This is especially true within the fractured region surrounding an excavation (Hildyard, 2001).

The problem of dynamic stability of excavations in rock is a multifaceted one and will not be fully understood for some time. However, data-bound problems are not the exception in rock mechanics, but the norm (Starfield and Cundall, 1988), and as explored here, application of and improvements to available numerical modeling tools may help incrementally advance the current state-of-the-art.

Figure 1 provides a diagram of the ways in which a numerical model may be used. As modeling software has become increasingly complex and computers increasingly powerful, there is a tendency in geomechanical modeling to move away from mechanism identification and qualitative parameter study, and toward site-specific prediction. However, in a data-limited field such as geomechanics, modeling is often more appropriately used as a tool for parameter study and identification of mechanisms (Starfield and Cundall, 1988). This is particularly true for very complicated rock engineering problems involving dynamics. This work takes the approach indicated by the left-hand side of Figure 1.

<b>Typical Situation</b>	Complicated geology, inaccessible; no testing budget	←-----→	Simple geology, \$\$\$ spent on site investigation
<b>Data</b>	NONE	←-----→	COMPLETE
<b>Approach</b>	Investigation of Mechanisms	←--- Bracket field behavior by parameter studies ---→	Predictive (direct use in design)

Figure 1: Spectrum of Modeling Situations (Itasca, 2015)

Simple models that capture mechanically significant features can often be very valuable. This approach to modeling in geomechanics has been advocated by Starfield and Cundall (1988), Barbour and Krahn (2004) and Hammah and Curran (2009). The incorporation of simple numerical modeling in mining engineering facilitates (Hammah and Curran, 2009):

- (i) Development of understanding,
- (ii) Proper formulation of questions,
- (iii) Reasonable approximation of behavior and provision of meaningful predictions, and
- (iv) Aids in the design of solutions and decision making.

This paper presents a fully-dynamic approach to modeling rock mass, which can be used to simulate

failure and ejection of rock material in the vicinity of an underground excavation. Application of this rock mass model to a typical hard rock mine drift is presented by Raffaldi and Loken (2016).

## 2. FULLY-DYNAMIC SIMULATION

To perform a dynamic analysis, it is first necessary to know the conditions acting on the excavation prior to loading it dynamically. Therefore, it is usually necessary to first develop a static model of the problem. The basic steps required to develop a static numerical model are:

- (i) Develop model geometry
- (ii) Discretize the model
- (iii) Assign constitutive models and material properties
- (iv) Apply appropriate boundary and initial conditions
- (v) Establish initial equilibrium in the model
- (vi) Perform an alteration to the model
- (vii) Solve for the solution
- (viii) Evaluate the results and revise model if necessary

Additionally, for a dynamic simulation, there are several further steps. These include:

- (ix) Evaluate wave transmission adequacy
- (x) Apply mechanical damping
- (xi) Apply dynamic boundary conditions
- (xii) Apply dynamic loading

Steps 7 and 8 must then be repeated for the dynamic solution.

### 2.1. ix – Evaluate Wave Transmission Adequacy

It is necessary to ensure that accurate wave transmission is achieved within the model. The main requirement is that the element sizes are small enough—with respect to the wavelength of the input wave—to ensure numerical accuracy. Kuhlemeyer and Lysmer (1973) demonstrated that the element size must be smaller than one-tenth to one-eighth of the wavelength associated with the highest frequency component in the modeled wave. In mathematical terms this means that:

$$\Delta l \leq \frac{\lambda}{10} \quad (1)$$

where,

$\Delta l$  = spatial element size, and  
 $\lambda$  = wavelength associated with the highest frequency component in the wave.

The wavelength is dependent on both the frequency of the wave and the material properties of the medium through which it propagates. The limiting wavelength can be determined from the wave velocities associated with the material with the least stiff elastic properties and the wave frequency via Equation 2:

$$\lambda = \frac{C}{f} \quad (2)$$

where,

$C$  = wave propagation velocity, and  
 $f$  = wave frequency

### 2.2. $x$ – Apply Mechanical Damping

Mechanical damping refers to a reduction in wave amplitude with vibration. Mechanical damping is the attenuation caused by energy dissipation associated with propagation through a medium, and is independent of attenuation due to geometric spreading. In a numerical model it is often necessary to explicitly simulate the natural energy dissipation, because without damping a system would oscillate indefinitely, and waves would propagate without attenuation (other than that due to geometric spreading). In numerical modeling of geomechanical systems, the goal is usually to simulate frequency-independent material damping to reproduce the energy losses in the natural system when subjected to dynamic loads (Itasca, 2015). The amount of damping that removes all oscillation in a system is known as critical damping. In structural systems, damping is usually between 2 and 10% of critical (Biggs, 1964). Damping in geologic materials is usually between 2 and 5% (Itasca, 2015). A lesser amount of damping (0.5% for example) may be required when additional damping from inelastic deformations such as plastic flow and slip along discontinuities is incorporated implicitly.

### 2.3. $xi$ – Apply Dynamic Boundary Conditions

Dynamic boundary conditions concern how stress waves behave at artificial boundaries. In geomechanical modeling, it is often necessary to artificially truncate boundaries of a model. In static analyses, displacement or stress boundary conditions can be prescribed at a distance from the area of interest sufficient to allow stresses to return to a virtually undisturbed state. In a dynamic analysis, these boundaries cause outward propagating waves to be reflected back into the model, when in reality, these waves would eventually attenuate as they continued onward through the earth. In numerical models, boundaries located far enough from the region of interest to allow material damping to dissipate the energy are usually not practical because of the large model dimensions that would be required. Therefore, viscous boundaries that absorb energy are usually applied along artificial boundaries to prevent reflection.

### 2.4. $xii$ – Apply Dynamic Loading

Dynamic loading deals with the transient loads that are applied during the simulation. The dynamic loading could be specified as either a transient stress, displacement, or velocity applied over some boundary of the model. For earthquake simulations, it could be a time

history of vertical and horizontal ground motion applied at the base of a model. For a problem concerning stability of an excavation in the presence of nearby blasting, a stress time-history representing the borehole pressure from a detonating explosive might be applied to an internal boundary within the model.

## 3. ROCK MASS MODEL

It was necessary for the rock mass model to be capable of both plastic deformations, and rock fracture and ejection. In order to accomplish this, the numerical code UDEC (Universal Distinct Element Code) (Itasca, 2015) was chosen. This program is based on the distinct element method and is useful when a continuum analysis fails to reproduce key mechanisms. In UDEC, the rock mass is represented as an assemblage of discrete blocks. These blocks are represented as a finite difference grid and subdivided into elements that individually deform in response to the applied forces or boundary constraints according to a prescribed linear or non-linear stress-strain law. UDEC allows finite displacement and rotations between discrete blocks, including complete detachment, and it is capable of recognizing new contact surfaces automatically during the simulation.

### 3.1. Conceptual Development

The rock mass model developed in UDEC is composed of three different parts: (1) the joints, (2) the joint force-displacement model, and (3) the constitutive model. These three parts act together to determine the overall rock mass behavior, and the joints allow discrete rock blocks to fracture and dislodge. The joint model governs the behavior of these joints, and the constitutive model governs the behavior of the intact rock between the joints. The overall objectives of the model are to allow the rock mass to:

- (i) Fail and deform in a ductile manner under high confinement,
- (ii) Fail in a brittle manner under low confinement,
- (iii) Fracture and allow discrete rock blocks to detach from the rock mass under static and dynamic loading, and
- (iv) Transmit elastic waves without distortion.

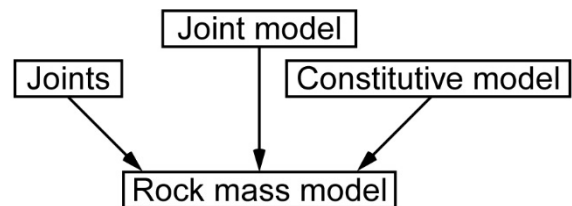


Figure 2: Conceptual diagram of rock mass model

### 3.2. Rock mass Jointing

The purpose of the joint system is not to represent actual rock structure, but to allow a pathway for the rock to

fracture. A randomized joint pattern was applied to the test samples via a Voronoi tessellation joint-generator embedded within UDEC. This joint system results in a distinct element model consisting of a finite set of distinct blocks. The contacts between the blocks are treated as boundary conditions and behave according to the prescribed joint model and associated joint properties. The block model used for the simulations is shown in Figure 3.

The Voronoi joint-generator used to create the distinct element block model requires several statistical inputs that control the average size and distribution of the blocks. UDEC defaults were used for most of these properties. Only the average edge length (0.25 m) and the Voronoi seed value were specified. The Voronoi seed value controls the starting point for the Voronoi tessellation. Changing the seed value will result in a similar but unique set of randomized joints. Other parameters were left as defaults but control additional properties such as block size uniformity.

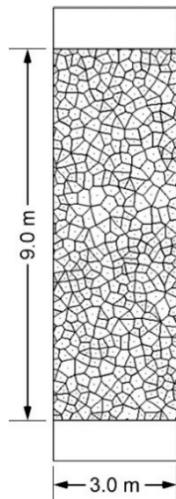


Figure 3: Model with Voronoi Joints

Stability and efficiency of UDEC models are sensitive to the specified minimum edge length and rounding length of block corners and the relationship between these two parameters. Edge length refers to the maximum length of a distinct element block that can be created in the model. Rounding length refers to the radius of rounded block corners. In UDEC, the rounding length can be at most half the minimum edge length. Careful selection of these properties is particularly important when using the Voronoi joint generator; even though a given pair of edge and rounding length values may satisfy the requirements of the program, they may over constrain the Voronoi joint generator resulting in either a failed Voronoi tessellation or the generation of non-uniform, highly angular blocks. This leads to extreme sensitivity of the model results to the Voronoi seed number. For the modeling described here, the block properties are provided in Table 1.

### 3.3. Joint Model

The area-contact model specified for the joints uses a linear approximation of joint stiffness and a Mohr-Coulomb slip criterion. Model parameters include shear and normal stiffness; frictional, cohesive, and tensile strength; and dilation angle. This model is well suited for simulating tightly packed rock blocks in area contact (as opposed to point contact) (Itasca, 2015).

Table 1: Block and Voronoi Tessellation Properties

Property	Units	Value
Block Minimum Edge Length	m	0.025
Block Rounding Length	m	0.010
Overlap Tolerance	m	0.050
Voronoi Joint Average Edge Length	m	0.250
Voronoi Joint Seed Value	n/a	2

In addition, strength values weaken with inelastic displacement to residual values. Blocks may detach, translate, rotate and collide with other blocks.

### 3.4. Constitutive Model

An isotropic Mohr-Coulomb strain-hardening/softening model with tension cutoff was chosen to simulate block deformability. During yield the material may either strain-harden or strain-soften by varying the strength properties as a function of plastic strain.

### 3.5. Material Properties

The material properties for both the constitutive model and joint model are provided in Tables 2 and 3. The properties are defined in such a way that the failure occurs through the solid when the rock is confined, but through the joints when unconfined.

For the solid, 90% cohesion is lost linearly through the first 4% of plastic strain. No other parameters changed with plastic strain, and the tension cutoff was set to a very large value to force tensile failure to occur through the joints.

Table 2: Constitutive Model Material Properties

Parameter	Units	Value
Density	kg/m <sup>3</sup>	2700
Bulk Modulus	GPa	29.2
Shear Modulus	GPa	13.5
Peak Cohesion	MPa	16
Residual Cohesion	MPa	1.6
Peak Friction Angle	Deg.	32
Residual Friction Angle	Deg.	32
Peak Tensile Strength	MPa	∞

Residual Tensile Strength	MPa	n/a
---------------------------	-----	-----

Joint stiffness properties were assigned values such that they had a minimal effect on the overall elastic modulus of the modeled rock mass. A tensile strength of 0.5 MPa was specified with a residual strength of zero. This means that once the joint strength is exceeded in either shear or tension, it retains no tensile resistance. The reduction occurs in a single step.

Table 3: Joint Model Material Properties

Parameter	Units	Value
Normal Stiffness	GPa/m	292
Shear Stiffness	GPa/m	135
Peak Cohesion	MPa	16
Residual Cohesion	MPa	n/a
Peak Friction Angle	Deg.	32
Residual Friction Angle	Deg.	n/a
Peak Tensile Strength	MPa	0.5
Residual Tensile Strength	MPa	0

#### 4. STATIC BEHAVIOR

A series of standard direct tension and compression tests were modeled using the Voronoi-joint rock mass, to evaluate its behavior under simplified loading conditions. Also, these models were used to perform a partial sensitivity analysis on the joint and constitutive properties in order to better understand the model.

##### 4.1. Uniaxial Tensile Test

To examine the behavior of the material in tension, a uniaxial tension test was simulated. The resulting stress-strain behavior is shown in Figure 4. It is observed that the material deformed linearly, reached a peak value and then failed in a brittle manner. A tensile crack formed perpendicular to the direction of loading, and no shear failure of any zones in the model was observed. The average vertical stress at failure for the numerical test was approximately 0.29 MPa.

Additionally, the overall elastic modulus of the material (measured as the slope of the stress-strain curve) is 22 GPa. This value is less than the elastic modulus assigned to the model zones. This reduction in overall modulus occurs as a result of the presence of the joints. Although the joints were assigned high stiffness values, they still contribute to the overall deformability of the rock mass because of the close joint spacing. Therefore, the rock mass modulus is a value that must be calibrated by adjusting the elastic moduli and the joint normal and shear stiffness to obtain the desired value.

##### 4.2. UCS and Triaxial Compression Tests

Next, a series of uniaxial and triaxial tests were simulated using the numerical properties listed in Table 2 and Table 3. This consisted of compression tests performed at confining pressures of 0, 2, 4, 6, 8, and 10 MPa. Figure 5 provides the resulting stress-strain relationships for these different tests. It is observed that with an increase in confining pressure, there is a corresponding increase in peak and residual strength as well as a decrease in the unloading modulus.

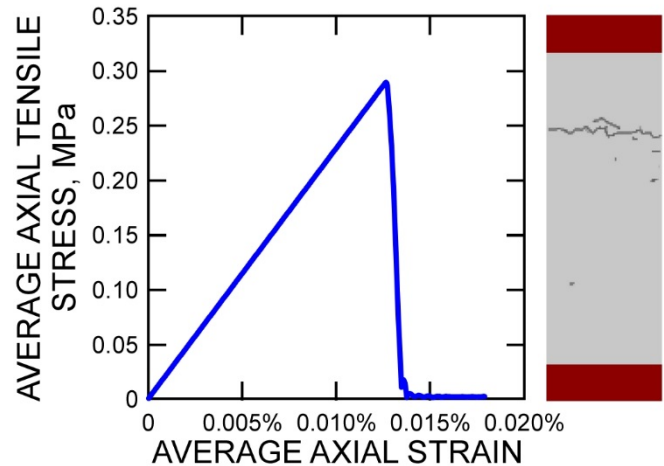


Figure 4: Modeled Direct Tension Test Results

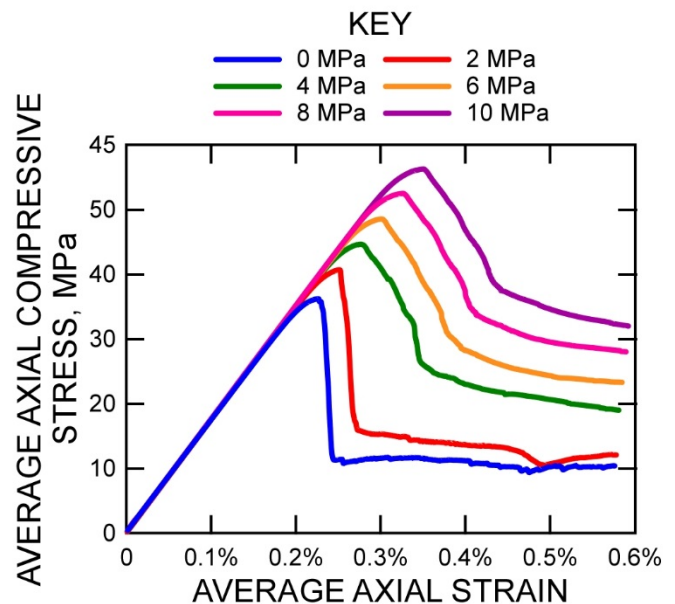


Figure 5: Modeled Compression Test Results (color indicates confinement pressure).

Figure 6 shows the plastic state and the velocity vectors at the end of the test for confining pressures of 0, 4, and 8 MPa. For the unconfined test, a shear fracture is observed, but also significant tensile cracking. The confined tests show a much more clearly defined shear failure and the tensile cracks are less developed.

Figure 7 shows gridpoint velocity vectors at the end of the simulation. It is observed that while the confined tests have split into two halves with well-defined shear planes, the unconfined model is both shearing and pulling apart in tension along the fractures.

## 5. DYNAMIC BEHAVIOR

Once the static behavior of the Voronoi rock mass model was validated, it was necessary to also investigate the dynamic behavior. Due to the presence of the Voronoi joints, there was concern for the ability of the rock mass model to transmit an elastic stress wave across these joints when they are intact. Several models were developed in order to pass simple one-dimensional compression and shear waves through the model and evaluate various parameters and material response.

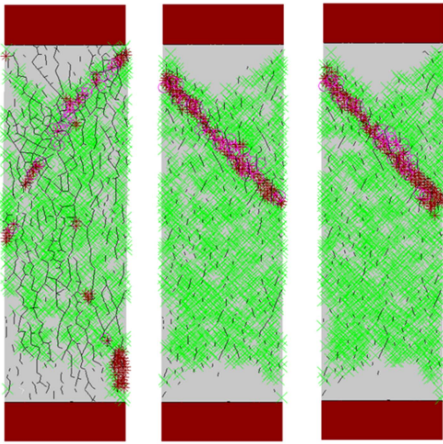


Figure 6: Zone Shear Failure for Compression Test with Confining Pressures of (a) 0 MPa, (b) 4 MPa, and (c) 8 MPa

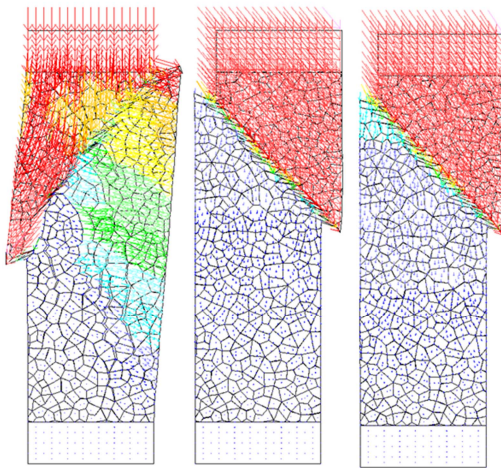


Figure 7: Velocity Vectors for Compression Test with Confining Pressures of (a) 0 MPa, (b) 4 MPa, and (c) 8 MPa

### 5.1. One-Dimensional Wave Propagation

A simple model was developed consisting of an elastic bar; one half was assigned steel properties while the

other was assigned aluminum properties. The modeled bar was 2 m thick by 500 m long. (Although the term *bar* is used, the model assumes plane strain in the out-of-plane direction.) Triangular elements with a maximum edge length of 0.3 m were used in both sides of the bar. The bar was constrained against vertical movement along its length. Viscous boundary conditions were applied along both ends of the bar to absorb the reflected wave on the left side, the transmitted wave on the right side, preventing the waves from being reflected back into the model. The loading was specified as a transient normal stress applied along the left end of the model. A conceptual diagram of the model is provided in Figure 8.

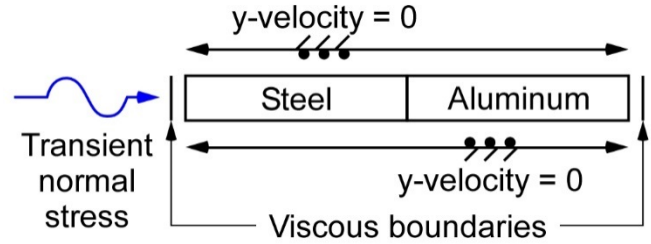


Figure 8: One-Dimensional P-Wave Propagation Model

To verify the model, the results are compared to the experimental work of Johnson (2010) and to the analytical solution for the amplitudes of transmitted and reflected waves for an incident wave provided by Jaeger et al. (2007) which states that:

$$\frac{A_t}{A_i} = \frac{2Z_1}{Z_1 + Z_2} \quad (3)$$

$$\frac{A_r}{A_i} = \frac{Z_1 - Z_2}{Z_1 + Z_2} \quad (4)$$

where,

- $A_i$  = amplitude of incident wave
- $A_t$  = amplitude of transmitted wave
- $A_r$  = amplitude of reflected wave
- $Z_1$  = acoustic impedance of medium 1
- $Z_2$  = acoustic impedance of medium 2

and for a p-wave,

$$Z_p = \rho C_p = \sqrt{\rho M_p} \quad (5)$$

where

- $Z_p$  = acoustic impedance for p-wave
- $\rho$  = density of medium
- $C_p$  = p-wave speed for medium
- $M_p = K + 4G/3 =$  constrained modulus

The steel and aluminum sections of the model were assigned the same material properties as in Johnson's experiment. In order to calibrate his testing apparatus, Johnson passed a strain wave with an amplitude of approximately 0.0027 through a steel incident bar into an aluminum bar and recorded the amplitude of the

reflected and transmitted wave after the wave passed across the steel/aluminum interface.

Table 4. Steel and Aluminum Elastic Properties

Material	Density	Young's Modulus	Poisson's Ratio
Viscomax 350 Steel	8.08 g/cm <sup>3</sup>	200 GPa	0.30
Aluminum 7075-T6	2.81 g/cm <sup>3</sup>	71.7 GPa	0.33

The peak particle velocity (PPV) to be applied in the model can be determined from the peak amplitude of the strain wave using Equation 6:

$$v(t) = C\varepsilon(t) \quad (6)$$

where,

$v(t)$  = particle velocity as function of time,  
 $C$  = wave speed for the medium, and  
 $\varepsilon(t)$  = particle strain as function of time

This can easily be converted to a stress input using Equation 7:

$$\sigma(t) = 2\rho Cv(t) \quad (7)$$

where,

$\sigma(t)$  = particle stress as a function of time  
 $\rho$  = material density  
 $C$  = wave speed for the medium  
 $v(t)$  = wave particle velocity as a function of time

Equation 5 may be used for either a p- or an s-wave. Note that the constant of '2' in the equation is a numerical requirement resulting from the application of the stress history across a viscous boundary condition (Itasca, 2015).

A single pulse with a frequency of 100 Hz was applied to the steel on the left side of the bar. Although this wavelength is much larger than that which was produced in Johnson's experiment, the peak strains (amplitudes) of the reflected and transmitted waves at the steel/aluminum interface are solely functions of the material properties (equations 4–6).

The results of the simulated test are presented in Table 5 with those from the analytical calculation and the laboratory experiment performed by Johnson (2010). It is observed that the numerical and analytical solutions are in agreement within six percent. The experimental results differ by more due to measurement error and energy losses in the system. The modeled incident, reflected, and transmitted waves are shown in Figure 9.

Table 5. Comparison of Modeled and Experimental Incident, Reflected and Transmitted Strain Waves

Value Type	Incident Strain-Wave Amplitude	Reflected Strain-Wave Amplitude	Transmitted Strain-Wave Amplitude

Lab	0.0027	-0.0013	0.0036
Analytic	0.002700	-0.001240	0.003940
Model	0.002700	-0.001235	0.003692

## 5.2. Response of a Single Joint

A model was then constructed to investigate the way that the intact joints behave when a wave is passed across them. This is important because the joints were intended to allow the rock to fracture, not to represent actual discontinuities in the rock. Therefore, it was imperative that their effect on wave propagation be minimal prior to fracture. The model used was similar to that of the one presented in Section 3, except that the entire bar was assigned the elastic properties used for the rock mass model (Table 2), and a single vertical joint was placed in the center of the bar with the same properties as listed in Table 3.

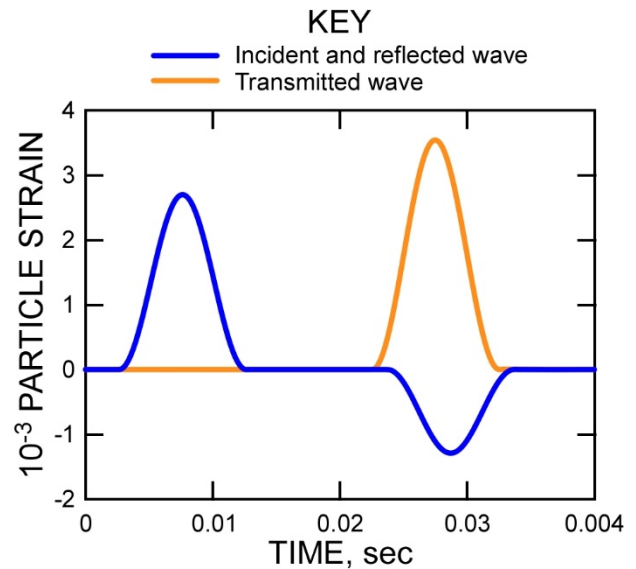


Figure 9: Incident, Reflected and Transmitted Wave for One-Dimensional Wave Propagation Test Model.

The joint was first modeled as elastic with infinite strength in order to simulate the case in which the strength of the joint was not exceeded. Later the joint was assigned a Mohr-Coulomb failure criterion with a tensile strength cutoff to verify its strength. Figure 10 shows a schematic of the model geometry and boundary conditions.

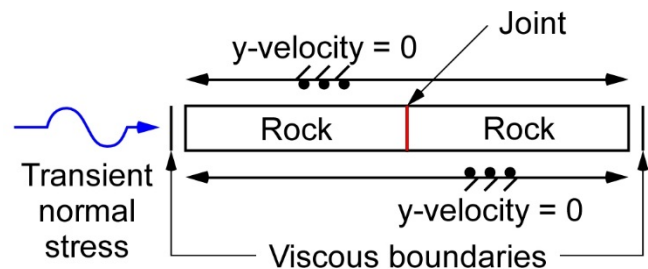


Figure 10: One-Dimensional P-Wave Propagation Model for Investigation of Behavior of a Single Joint.

A single pulse was propagated across the joint. Again, strain histories were recorded on each side of the bar. Figure 11 shows the velocity histories measured on each side of the bar and verifies that the compression wave passes through the joint virtually unaltered. The joint angle was changed to  $45^\circ$  to check if the angle of incidence had any effect on wave transmission. A virtually identical result was achieved.

Next, the model was reconfigured so that a shear wave could be propagated through it. This is accomplished by fixing the bar in the direction parallel to the direction of wave propagation, allowing the bar to deform in the vertical direction. A conceptual depiction of this model is provided in Figure 12.

A shear wave was propagated across the joint and velocity histories were recorded on each side. The wave was again observed to be virtually unaltered on both sides of the joint.

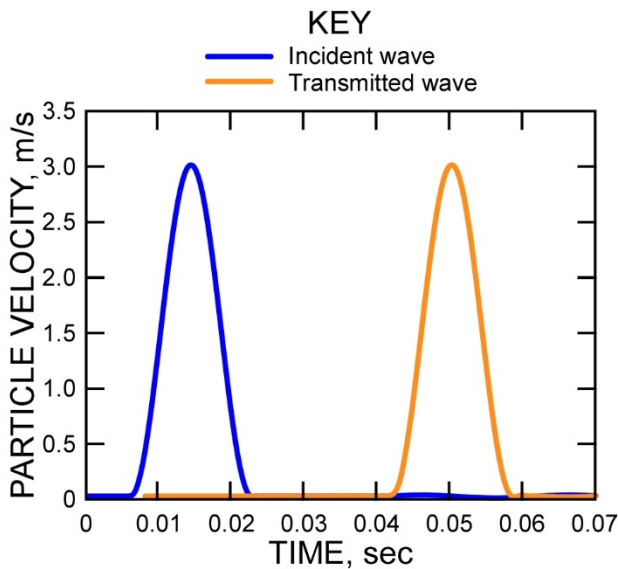


Figure 11: Incident and Transmitted wave across a single joint with no joint failure.

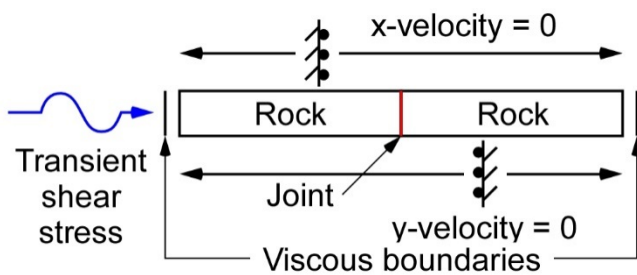


Figure 12: One-Dimensional S-Wave Propagation Model for Investigation of Behavior of a Single Joint.

The joint was then changed to a Mohr-Coulomb model with a friction angle of zero and cohesion of 16 MPa. A shear wave with a peak stress of around 36 MPa was applied to the bar. The joint was observed to fail in shear as the wave passed, allowing only a portion of the wave to transmit through the joint. The peak stress transmitted

to the other half of the bar was found to be almost exactly 16 MPa. Figure 13 shows a plot of the stress histories recorded on the two sides of the joint.

Two experiments were performed to test joint tensile strength. In the first, a tensile stress was applied. In the second, tension was generated by reflection of a compression wave, which was accomplished by removing the viscous boundary condition on the right end of the bar. In both cases, the bar was split into two halves at the joint.

### 5.3. Elastic Wave Propagation

Aluminum parameters used in Section 4.1 were replaced with the Voronoi rock mass model parameters from Sections 2 and 3. Compression and shear waves were propagated through the material. Initially, peak particle velocities were limited to avoid failure. A schematic of the model is provided in Figure 14.

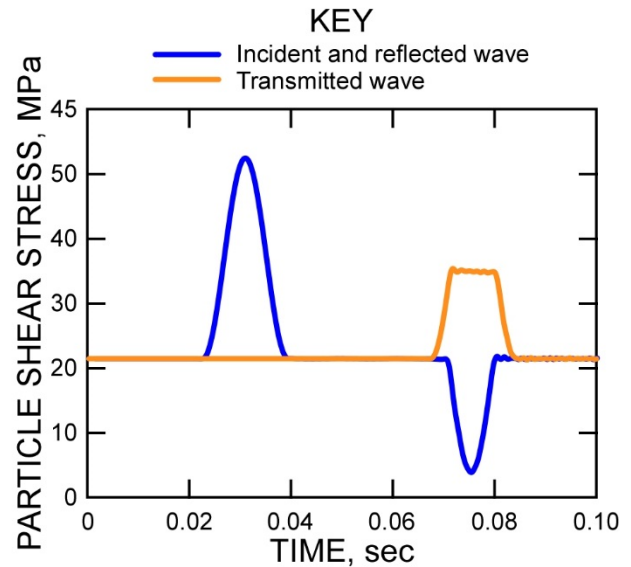


Figure 13: Incident, Reflected and Transmitted Wave across a single joint with no joint shear failure.

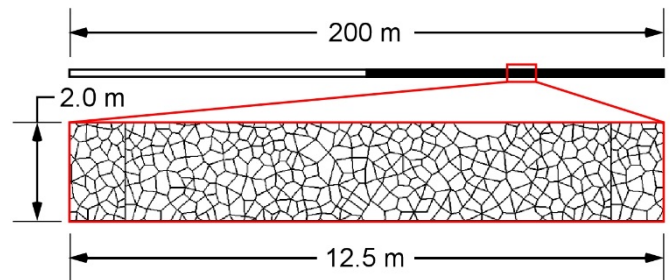


Figure 14: Diagram of one dimensional wave propagation model for Voronoi rock mass model.

Velocity histories were recorded at three locations. One history was recorded in the steel incident bar and two on the right and left ends of the Voronoi rock mass. The two points in the Voronoi rock material were used to compute the wave speeds. Elastic properties were

computed from the calculated wave speeds using Equations 8 and 9 (Kolsky, 1963).

$$C_p = \sqrt{\frac{K + 4G/3}{\rho}} \quad (8)$$

$$C_s = \sqrt{\frac{G}{\rho}} \quad (9)$$

where,

$C_p$  = p-wave speed

$C_s$  = s-wave speed

$K$  = Bulk Modulus

$G$  = Shear Modulus

$\rho$  = material density

The damping ratio of the material (if any) is computed based on the amplitude decay between the two measurement points. Table 6 provides the calculated p- and s-wave propagation speeds in the Voronoi rock material; also, the Young's modulus, Poisson's ratio, and damping ratio which were computed from these speeds.

Table 6. Dynamic Properties Calculated in the Model

Property	Value
p-wave speed (m/s)	3048
s-wave speed (m/s)	1778
$C_p/C_s$	1.71
Young's Modulus (GPa)	22.9
Poisson's Ratio	0.24
Damping Ratio	0%

The calculated properties are within 5% of the static values. It is important to note that these properties are not necessarily the true material properties of the modeled material, and this calculation was performed simply as an exercise to verify that the wave transmission in the jointed model was appropriate. The Young's modulus calculated for the Voronoi rock mass material during the simulated UCS and triaxial compression tests was 22.1 GPa. The back-calculated modulus based on the measured wave speed is 22.9 GPa. Based on the propagation speed, the wavelength associated with the frequency of the applied stress wave, the decrease in amplitude between the two histories, and distance between these history locations, the damping ratio for the Voronoi rock material was found to be negligible. However, this is only for the set of joint properties used in this work. Raffaldi (2015) observed a damping ratio of 4% for a similar model based on coal material properties in which the joints stiffness values were lower.

#### 5.4. Dynamic Fracture of a Single joint

PPV is usually the wave parameter chosen for correlation with rock mass damage because it directly corresponds to stress in a constrained medium (Edwards and Northwood, 1960; Duvall and Fogelson, 1961). However, the mechanical behavior of a solid in the vicinity of an unconstrained surface (such as an underground excavation) is different. For a wave of fixed PPV, the associated accelerations will increase linearly with increasing wave frequency. The peak particle acceleration (PPA) associated with a 60 Hz wave of the form:

$$v(t) = (0.5)PPV[1 - \cos(2\pi ft)] \quad (10)$$

where,

$v(t)$  = velocity as a function of time

PPV = peak particle velocity

$f$  = frequency

$t$  = time

will be three times greater than that of a 20 Hz wave. This is evident after taking the derivative of Equation 10 with respect to time to obtain the acceleration function shown in equation 11.

$$a(t) = PPV(\pi f) \sin(2\pi ft) \quad (11)$$

where,

$a(t)$  = acceleration as a function of time

and all other parameters have been previously defined.

Further, because force is proportional to the product of mass and acceleration, it is expected that accelerations are also important to understanding the mechanics of dynamic rock damage and failure.

A model was developed that consisted of a single block attached at the end of a bar. Both the block and the bar were elastic and of the same material (as described in Section 3.5). A vertical joint separated the bar from the block and was assigned a tensile strength ranging from zero to infinity. A schematic is shown in Figure 16.

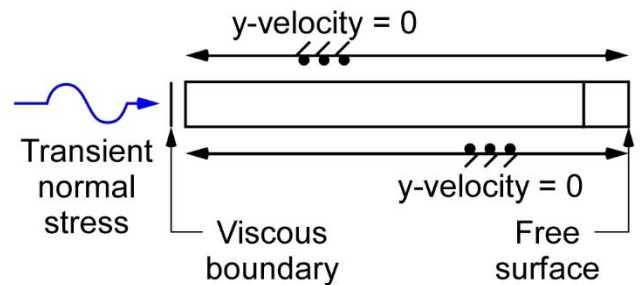


Figure 16: One-Dimensional S-Wave Propagation Model for Investigation of Behavior of a Single Ejecting Block

A single-pulse compression wave with a PPV of 3 m/s was propagated along the bar, across the joint, and allowed to reflect at the free surface. It was observed that, for a wave of any frequency, if the tensile strength

was infinite, the wave was simply reflected back as a tensile wave and the peak particle velocity measured at the free surface was 6 m/s. This value is exactly double that of the constrained wave, consistent with theory (Kolsky, 1963). Conversely, when the tensile strength of the joint was set to zero, the block ejected with a velocity of 6 m/s for all modeled frequencies. However, as the tensile strength of the joint was increased, the ejection velocity decreased.

For a given frequency, and a pulse shape of the form given in Equation 10, the ejection velocity will decrease from 6 m/s to 3 m/s as the tensile strength is increased. At some threshold value of tensile strength, the block will no longer eject. This threshold tensile strength increases linearly with frequency and is shown in Figure 17. The relationship between tensile strength and ejection velocity for 20, 40, and 60 Hz waves of PPV of 1, 2 and 3 m/s is shown in Figure 18.

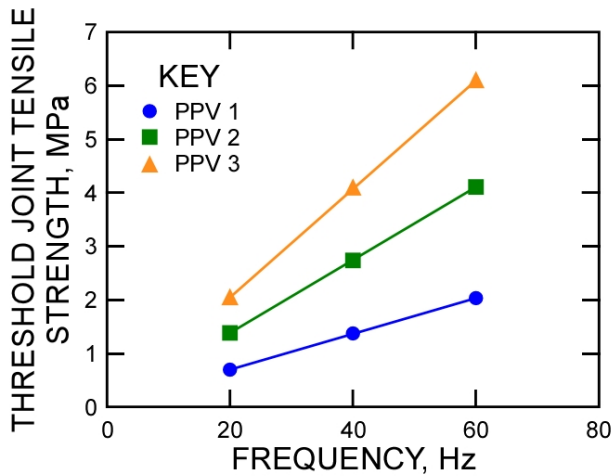


Figure 17: Relationship between frequency and joint tensile strength threshold.

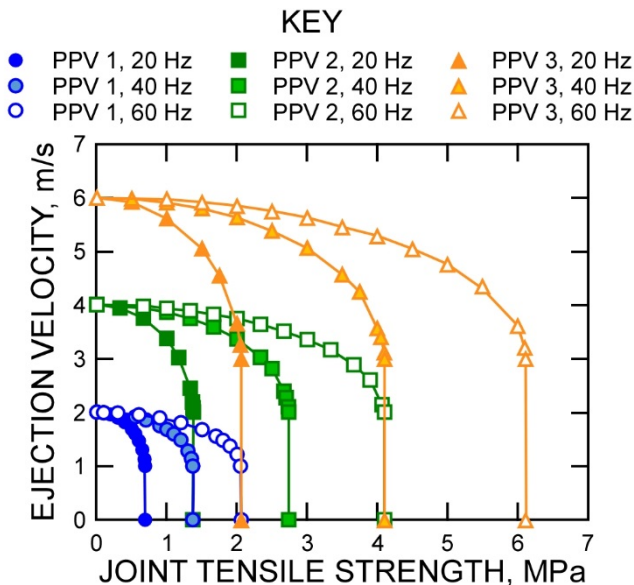


Figure 18: Relationship between ejection velocity and joint tensile strength for the modeled ejecting block

The PPA will occur where the slope of the velocity wave is steepest. If we consider the shape of the wave used, the maximum acceleration will occur when the velocity is half the peak value and will vary linearly with frequency. In this case PPA occurs at the quarter point of the period, or at  $t = 0.25/f$ . The greater the frequency, the steeper the slope, and the greater the peak acceleration. At the point of maximum velocity (PPV), the slope of the velocity wave is zero, and therefore the acceleration is also zero. In between these extremes the acceleration will increase from zero to its maximum (the PPA) which will depend linearly on frequency.

The value of acceleration at which the block ejected is plotted for all three frequencies and PPVs (Figure 19). The relationship between joint strength and acceleration required to cause failure is linear for an ejecting block of fixed mass. That is, for a given joint tensile strength, there is a threshold value of acceleration that will cause failure, independent of frequency and PPV. This result indicates that acceleration, not velocity, is the key factor in understanding rock ejection during seismic loading.

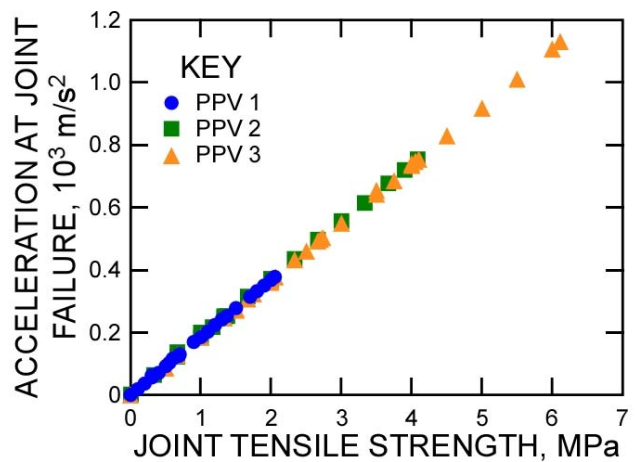


Figure 19: Relationship between particle acceleration at joint failure and joint tensile strength for the modeled ejecting block.

Fracturing in confined portions of the rock mass from excess stress levels, on the other hand, is more directly related to PPV as the stress that develops in an axially confined portion of the bar is proportional to velocity and not acceleration. Because the stress in a *confined* medium is due simply to the strains that develop in the material as the wave passes, the peak stress does not depend on acceleration. However, at an *unconfined* surface, there is no longer any material to produce a compressive reaction force, and a tensile force develops on the joint that is equal to the product of the mass and the acceleration of the block that is attempting to detach. The force required to detach the block from the rest of the rock mass is equal to the area of the joint times the joint strength. In Figure 20, the accelerations that caused joint failure for all of the cases in Figure 19 are

multiplied by the mass of the block, and plotted versus the force required to cause joint failure. It is seen that for a block near a free surface, the acceleration accounts for all of the force required to fracture the joint.

### 5.5. Dynamic Failure

Lastly, the model used in Section 5.3 was altered so that a p-wave with a PPV of 3 m/s was applied. Based on the equation developed by Kaiser et al. (1996), this is approximately equivalent to the PPV at a distance of 20 m from a mining induced seismic event of magnitude 3.0. This is large enough to cause significant damage to underground excavations. The wave was propagated through the model and the right end of the bar was left unconstrained so that the wave could cause damage.

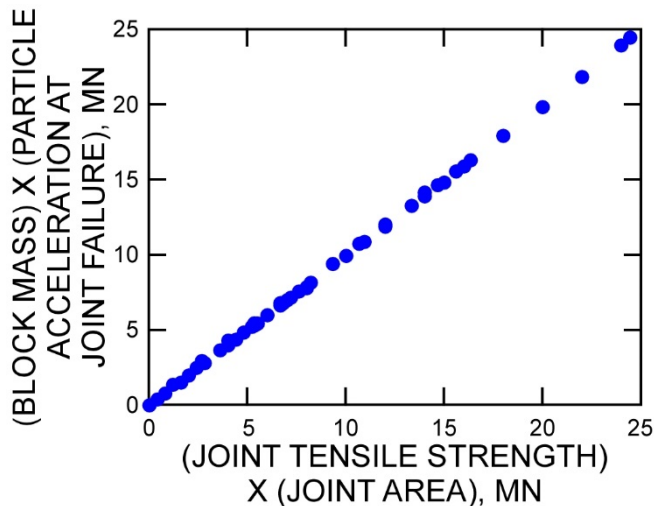


Figure 20: Relationship between the product of block mass and block acceleration and the product of joint tensile strength and joint area

The unconstrained end of the bar was ejected to the right during the simulation. Figure 21 shows the velocity vectors and damage that occurred for a joint tensile strength of zero. The width of the ejected area corresponded with exactly one-half of the wavelength associated with the propagating wave. Further, the peak ejection velocity was equal to twice the PPV of the wave, corresponding to the doubling of the velocity at a free surface.

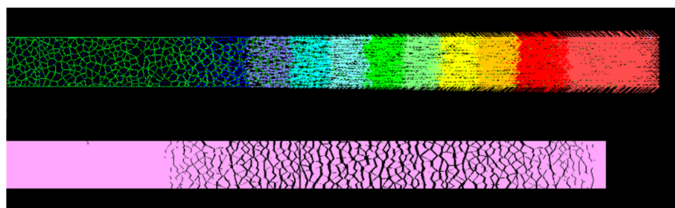


Figure 21: Velocity Vectors and Joint Opening for One-Dimensional Wave Propagation in Rock Mass Model with no tensile strength

The ejection velocity was observed to decrease with distance into the rock bar. The ejection velocity and the damaged length of bar was also observed to decrease

with increasing joint tensile strength. However, the relationship between the wave parameters and damage is more complicated and the absence of confinement with distance from the free surface prevents any meaningful results from being extracted. A two-dimensional (2-D) simulation with appropriate in situ stresses is required.

## 6. CONCLUSIONS

Based on the simulated quasi-static and dynamic experiments, the Voronoi joint rock mass model is appropriate for use in mechanism-based dynamic simulations involving rock fracture and ejection. The model behaves reasonably under both static and dynamic loading. It is also capable of accurate wave propagation. Significant understanding of the dynamic simulation process was achieved as well as a better understanding of wave propagation and dynamics in general. The rock mass model presented in this work has the ability to:

- (i) Fail and deform in a ductile manner under high confinement,
- (ii) Fail in a brittle manner under low confinement,
- (iii) Fracture and allow discrete rock blocks to detach from the rock mass under both static and dynamic loads, and
- (iv) Transmit elastic waves without distortion.

This preliminary one-dimensional investigation, provides insight into the dynamic failure of rock materials. It shows that the stresses induced in the rock near a free surface during dynamic loading are significantly different than those that occur within a constrained solid. In the vicinity of an unconstrained surface, the accelerations associated with a seismic wave are important to understanding rock fracture and ejection. Forces develop along planes of weakness that are equal to the product of the mass and acceleration of the rock block attempting to eject. For a seismic wave of given PPV, higher frequencies will be associated with higher accelerations and have the potential to be more damaging to a rock surface.

The main objective of this work was to develop a model which could be used for further study and to better understand the physics associated with dynamic rock damage. It is acknowledged that one of the limitations of this rock mass model is that it is based only on static material properties, and it is well known that many materials, including rock, exhibit different strength behavior under static and dynamic loading. However, dynamic behavior of rock is difficult to quantify and to do this would require considerable rock and site information. Therefore, incorporating such complexity is, at this time, beyond the scope of this work.

Despite this limitation, this rock mass model can be used to further investigate the stability of underground openings subjected to ground vibrations. In the future,

this basic methodology can be adapted and modified to incorporate specific joint patterns, more complex material and joint models, and etc., as needed. The beginnings of such work is presented in a companion paper that applies this method to a 2-D excavation model (Raffaldi and Loken, 2016).

## DISCLAIMER

The findings and conclusions in this paper have not been formally disseminated by the National Institute for Occupational Safety and Health and should not be construed to represent any agency determination or policy.

Mention of any company or product does not constitute endorsement by the National Institute for Occupational Safety and Health.

## REFERENCES

- Ansell, A. 2005. Laboratory testing of a new type of energy absorbing rock bolt, *Tunneling and Underground Space Technology* 20, pp. 291–300.
- Ansell, A. 2006. Dynamic testing of steel for a new type of energy absorbing rock bolt, *Journal of Constructional Steel Research* 62, pp. 501–512
- Barbero, M., G. Barla and A. Zaninetti. 1996. Dynamic shear strength of rock joints subjected to impulse loading. *International Journal of Rock Mechanics and Mining Science*, 33(2), 141–151.
- Barbour, S.L. and J. Krahn. 2004. Numerical Modeling Prediction or Process? *Geotechnical News*, 44–52.
- Biggs, J.M. 1964. *Introduction to Structural Dynamics*. McGraw Hill. New York, NY.
- Duvall, W.I., and D.E. Fogelson. 1961. Review of criteria for estimating damage to residences from blasting vibrations. *Bureau of Mines RI 5968*, 1–46.
- Edwards, A. T. and T.D. Northwood. 1960. Experimental studies of the effects of blasting on structures. *The Engineer*.
- Hammah, R.E. and J.H. Curran. 2009. It is better to be Approximately Right than Precisely Wrong – Why Simple Models Work in Mining Geomechanics. Paper presented at the 43rd US Rock Mechanics Symposium, Asheville, NC.
- Hildyard, M.W. 2001 Wave interaction with underground openings in fractured rock, Ph.D. Thesis, University of Liverpool, 2001, 283 pp.
- Itasca Inc. 2015. Universal Distinct Element Code (UDEC v6.0). Itasca Consulting Group, MN.
- Jaeger, J.C., N.G. Cook and R.W. Zimmerman. 2007. *Fundamentals of Rock Mechanics*. 4th ed. Blackwell Publishing. Malden, U.S.A.
- Johnson, J.C. 2010. The Hustrulid Bar – A Dynamic Strength Test and Its Application to the Cautious Blasting of Rock. (Ph.D.) University of Utah, Salt Lake, UT.
- Kaiser P.K., D.D. Tannant and D.R. McCreath. 1996. *Canadian rockburst support handbook*. Sudbury, Ontario: Geomechanics Research Centre, Laurentian University.
- Kolsky, H. 1963. *Stress Waves in Solids*. Dover. New York, NY
- Kuhlemeyer, R.L. and J. Lysmer. 1973. Finite Element Method Accuracy for Wave Propagation Problems. *Journal of Soil Mechanics and Foundations Division of the American Society for Civil Engineers*, 99(SM5), 421–427.
- Mohamed, K.M., A.M. Yassien and S.S. Peng. 2006. Cementitious Plug Seal/Rock Interface under Static and Dynamic Loadings. *National Institute for Occupational Safety and Health (NIOSH)*. pp. 14.
- Qian, Q., C. Qi, and M. Wang. 2009. Dynamic strength of rocks and physical nature of rock strength. *Journal of Rock Mechanics and Geotechnical Engineering*. Vol. 1(1) pp. 1–10.
- Raffaldi, M.J. 2015. *Static and Dynamic Discrete Element Modeling of Slender Coal Pillars*, M.S. Thesis, University of Kentucky, 223 pp.
- Raffaldi, M.J. and M.C. Loken. 2016. Framework for simulating fracture, ejection, and restraint of rock around a mine drift subjected to seismic loading. Paper presented at the 50th US Rock Mechanics Symposium, Phoenix, AZ, 2016 (this conference).
- Starfield, A.M. and P.A. Cundall. 1988. Towards a methodology for rock mechanics modelling. *International Journal of Rock Mechanics and Mining Science*, 24(3): 99–106